Conference Paper

Effect of Water Permeability Reduction Index on Gas Production from Hydrate-bearing Clayey-Silt Sediments by Depressurization

X. L. Ma[1,2], B. Li[1,2,3], R. Jia[1,2], W. Guo[1,2], and Y. H. Sun[1,2]

[1]Construction Engineering College, Jilin University, Changchun, 130026, China
[2]Key Laboratory of Drilling and Exploitation Technology in Complex Condition, Ministry of Land and Resource, Changchun, 130026, China
[3]College of Environment and Resources, Jilin University, 130021, China

Corresponding Author:
Y. H. Sun
syh@jlu.edu.cn

Received: 14 September 2018
Accepted: 1 October 2018
Published: 14 October 2018

Publishing services provided by Knowledge E

Selection and Peer-review under the responsibility of the ASRTU Conference Committee.

Abstract

Gas hydrates in Shenhu area are mainly hosted in clayey-silt sediments, which will make its multiphase flow more complex. Therefore, they will have an impact on gas production from hydrate-bearing clayey-silt sediments. In this study, a two-dimensional model was used to evaluate the behavior of hydrate production by depressurization in site SH2, Shenhu area, with different values of water permeability reduction index *n*. The results show that with the increase of *n*, the water production and gas production have decreased significantly. When *n* increases from 2.5 to 4.5, V_G drops from 1.93×10^6 m^3 to 1.34×10^6 m^3, and V_W drops from 6.69×10^5 m^3 to 4.46×10^5 m^3.

Keywords: gas hydrate, numerical simulation, water permeability reduction index, clayed-silt sediments, Shenhu area

1. Introduction

Natural gas hydrate (NGH) is an ice-like crystalline compound formed by natural gas molecules and water molecules [1]. It is widely distributed in the permafrost regions and marine sediments, which is considered as one of the potentially clean future energy. According to preliminary estimates, the total amount of energy in natural gas hydrate is two times larger than that of conventional oil and gas resources [2].

There are four main methods for hydrate production: depressurization, thermal stimulation, inhibitor injection, and CO_2–CH_4 replacement [3]. On July 9, 2017, China successfully completed its first pilot production of marine hydrate by depressurization in the Shenhu area, northern South China Sea. It was the first time in the world to exploit hydrates hosted in the clayey-slit sediments [4]. The total volume of gas production was up to 3.09×10^5 m^3 in 60 days [4, 5]. Although this methane hydrate production has made a great progress, it is far from being commercialized.

Based on the data obtained from hydrate drilling expeditions in the South China Sea, a lot of numerical simulations were carried out. Su et al. [6] evaluated the production potential of hydrate reservoir at site SH3 by depressurization using a vertical well and investigated the sensitivity of hydrate exploitation under different bottom hole pressure, initial hydrate saturation, intrinsic permeability, and overburden's permeability. By using a single horizontal well in the middle of the HBL, which was set to constant pressure and temperature, the total gas production reached 3.46×10^4 m^3/d [7]. Jin et al. [8] investigated the enhancement of thermal simulation on gas production and they also studied the effects of different well placements on gas hydrate production. Sun et al. [9] studied gas and water production rate, geomechanical response under different conditions including hydrate saturation heterogeneity, hydrate formation permeability, and gas formation permeability. Konno et al. [10] simulated the first marine hydrate production in Japan through numerical simulation. The simulation results showed that the gas production gradually increased with the expansion of the decomposition area, and the increase of hydrate formation permeability increased the ratio of gas to water.

Gas hydrates in Shenhu area are mainly hosted in clayey-silt sediments, which will make its multiphase flow more complex. But the effects of water permeability reduction index *n* on gas hydrate production were poorly studied. So, the main purpose of this study is to evaluate the effects of different *n* on gas and water production.

2. Simulation Model

The schematic depiction of gas production from the hydrate reservoirs in site SH2 in this simulation is shown in Figure 1. This model is divided into three layers, which are permeable overburden, gas hydrate bearing-sediments (the GHBS), and permeable underburden. The hydrate reservoir thickness is assumed to be 40 m, the value of intrinsic permeability k_H is set to be 10 mD, the porosity of the GHBS is assumed to be 38%, and the average hydrate saturation is assumed to be 40% [11]. The thickness of the permeable overburden and the permeable underburden is set to be 30 m. The sediments lithology of overburden and underburden, such as permeability and porosity, are the same as the GHBS. The production well is in the center of this cylindrical hydrate reservoir with a radius of 0.1 m. Other properties and conditions related to the reference case are listed in Table 1. In this study, the perforation interval has a total length of *Lp* = 20 m, which is located in the middle of the GHBS. The production well has a constant pressure of 3 MPa.

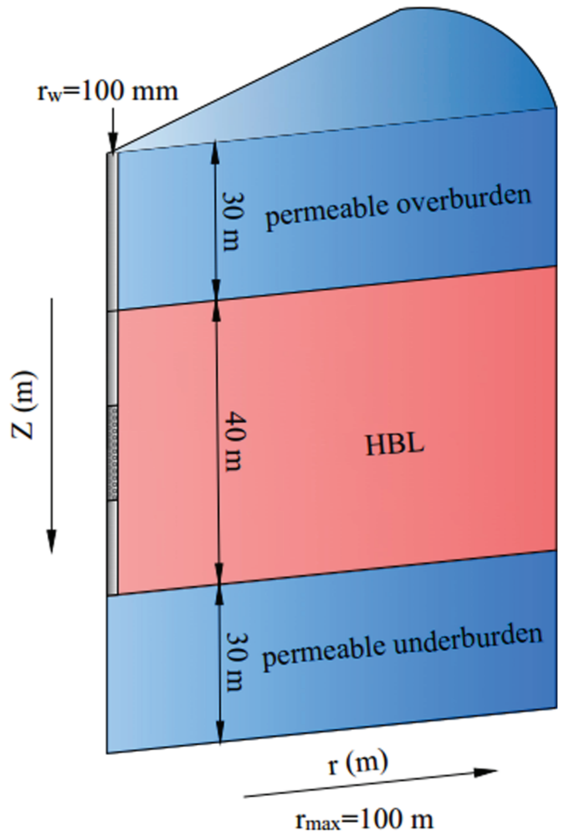

Figure 1: Schematic of simulated hydrate reservoir at site SH2.

The values of irreducible water saturation, irreducible gas saturation, and gas entry pressure are not fixed values; they will change with the particle size, clay content, and hydrate saturation. But in this simulation, those parameters are assumed to be fixed values. The relative permeability model used in this simulation is as follows [12]:

$$K_{rA} = \left(\frac{S_A - S_{\text{ir}A}}{1 - S_{\text{ir}A}} \right)^{\text{n}} \tag{1}$$

$$K_{rG} = \left(\frac{S_G - S_{\text{ir}G}}{1 - S_{\text{ir}A}} \right)^{\text{nG}} \tag{2}$$

$$K_{\text{r}H} = 0 \tag{3}$$

The capillary pressure function used is as follows [13]:

$$P_{\text{cap}} = -P_0 \left[\left(S^* \right)^{-1/\lambda} - 1 \right]^{1-\lambda} \tag{4}$$

$$S^* = \frac{S_A - S_{\text{ir}A}}{S_{mxA} - S_{irA}} \tag{5}$$

$$-P_{\text{max}} \le \text{P}_{\text{cap}} \le 0 \tag{6}$$

Table 1: Main hydrate deposit properties and conditions at site SH2.

Overburden thickness ΔZ_O	30 m
Underburden thickness ΔZ_U	30 m
GHBS thickness ΔZ_H	40 m
Completion interval (L_P)	20 m (in the middle of GHBS)
Borehole radius	0.1 m
Initial pressure P_B(at base of GHBS)	14.97 MPa
Initial temperature T_B(at base of GHBS)	14.87°C
Gas composition	CH_4
Porosity Φ (all formations)	38%
Initial saturation in the GHBS	S_A= 0.60, S_H= 0.40
intrinsic permeability $k_x = k_y = k_z$ = 10 mD (all formations)	10 md
water salinity (mass fraction)	3.05%
Grain density ρ_R (all formations)	2600 kg/m3
Dry thermal conductivity k_{dry} (all formations)	1.0 W/m/K
Wet thermal conductivity k_{wet} (all formations)	3.1 W/m/K
Composite thermal conductivity model	$k_\theta = k_{dry} + (\sqrt{S_A} + \sqrt{S_H})(k_{wet} - k_{dry}) + \phi S_I \lambda_I$
Capillary pressure model	$P_{\text{cap}} = -P_0 \left[(S^*)^{-1/\lambda} - 1\right]^{1-\lambda} S^* = \dfrac{S_A - S_{irA}}{S_{\text{mx}A} - S_{\text{ir}A}}$
λ	0.45
Relative permeability model	$k_{rA} = \left(\dfrac{S_A - S_{\text{irA}}}{1 - S_{\text{ir}A}}\right)^{\text{n}} k_{rG} = \left(\dfrac{S_G - S_{\text{irG}}}{1 - S_{\text{irG}}}\right)^{n_G}$
n	2.5/3.5/4.5
n_G	4.5

3. Results and Discussions

3.1. Spatial distributions of physical properties in reservoir

3.1.1. Spatial distributions of pressure (P)

Figure 2 shows the evolution of the pressure distribution over time in the entire formation with P_w = 3 MPa. From the Figure 2, we can know pressure distribution: (1) in the first ten days of production, the water near the production well flows into the production well under the pressure gradient, and the effect of the depressurization is only within 20 meters; (2) after 365 days, when the water from the overburden and underburden enters the production well; (3) in 10 years of production, the range of hydrate decomposition is within 30 meters.

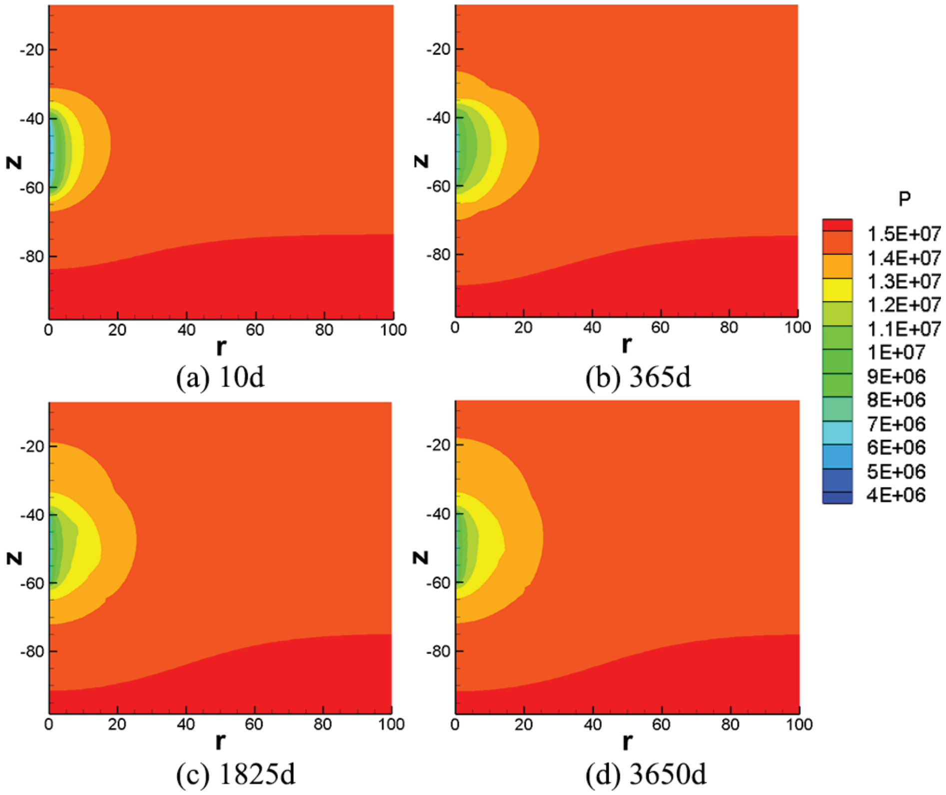

Figure 2: Evolution of pressure distribution at different time periods.

3.1.2. Spatial distributions of hydrate saturation (S_H)

The following conclusions results from Figure 3: (1) during the ten years of production, the range of hydrate decomposition is limited to 20 meters; The existence of hydrate reduces the effective permeability of clayey-slit sediments, which affects the range of the depressurization, and increases the time of gas flows to the production well; (2) in the 365th day, hydrate decomposition occurs at both the upper and lower boundaries of the GHBS, and the upper boundary of the GHBS decomposes rapidly, which is mainly caused by the high temperature fluid of the underburden and lower overburden flowing into production, and the temperature of the underburden is higher than that of overburden [7].

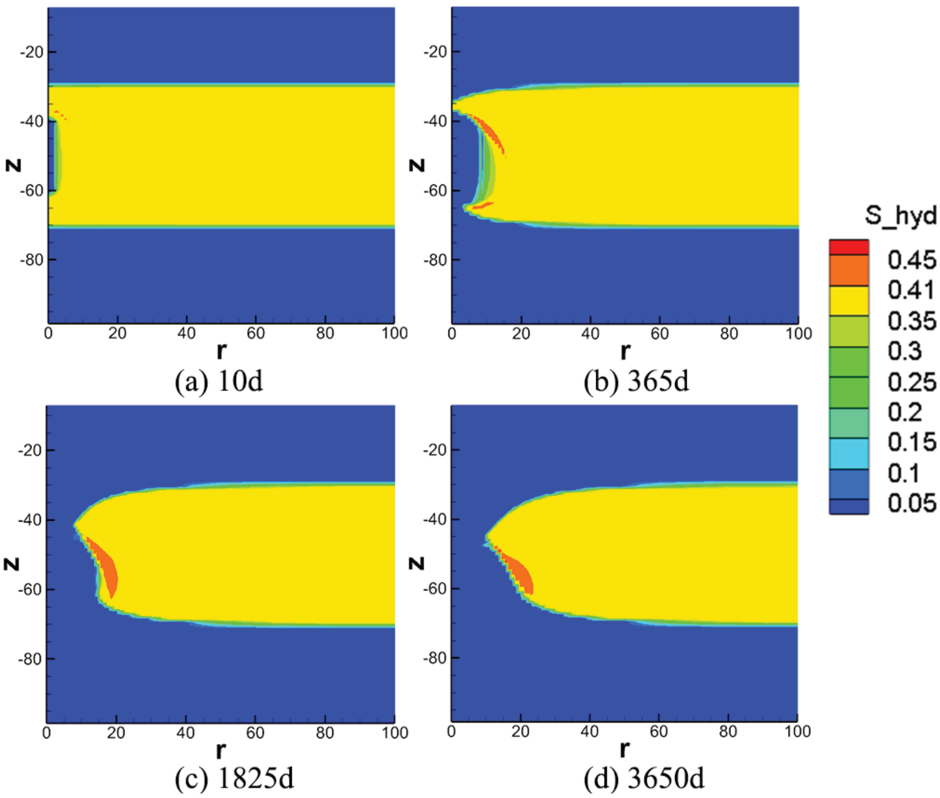

Figure 3: Evolution of hydrate saturation at different time periods.

3.1.3. Spatial distributions of gas saturation (S_G)

A number of characteristics can be concluded from Figure 4. The gas saturation in the whole process of production is below 0.2, and the gas saturation gradually decreases with the production. In the early stage of production, gas is mainly distributed around the production well, but when the water from the underburden and overburden flows into the production well, the gas is mainly distributed on the lower decomposition edge. It can be seen from Figure 4 that the range of gas is larger than hydrate decomposition area, which confirms the reason for the formation of secondary hydrate.

3.2. Gas production and water production behaviors

As shown in Figure 5, there are many significant changes in three cases of different *n*. As *n* increases, the total gas production rate Q_G and water production rate Q_W gradually decrease. The reason is that the relative permeability of gas and water decreases rapidly with the decrease of saturation in higher *n*. And it is noticeable that Q_G declines rapidly at the initial stage, then slows down gradually, and finally keeps stable. In the whole production, when the values of *n* are equal to 2.5, 3.5, and 4.5, Q_G decreases

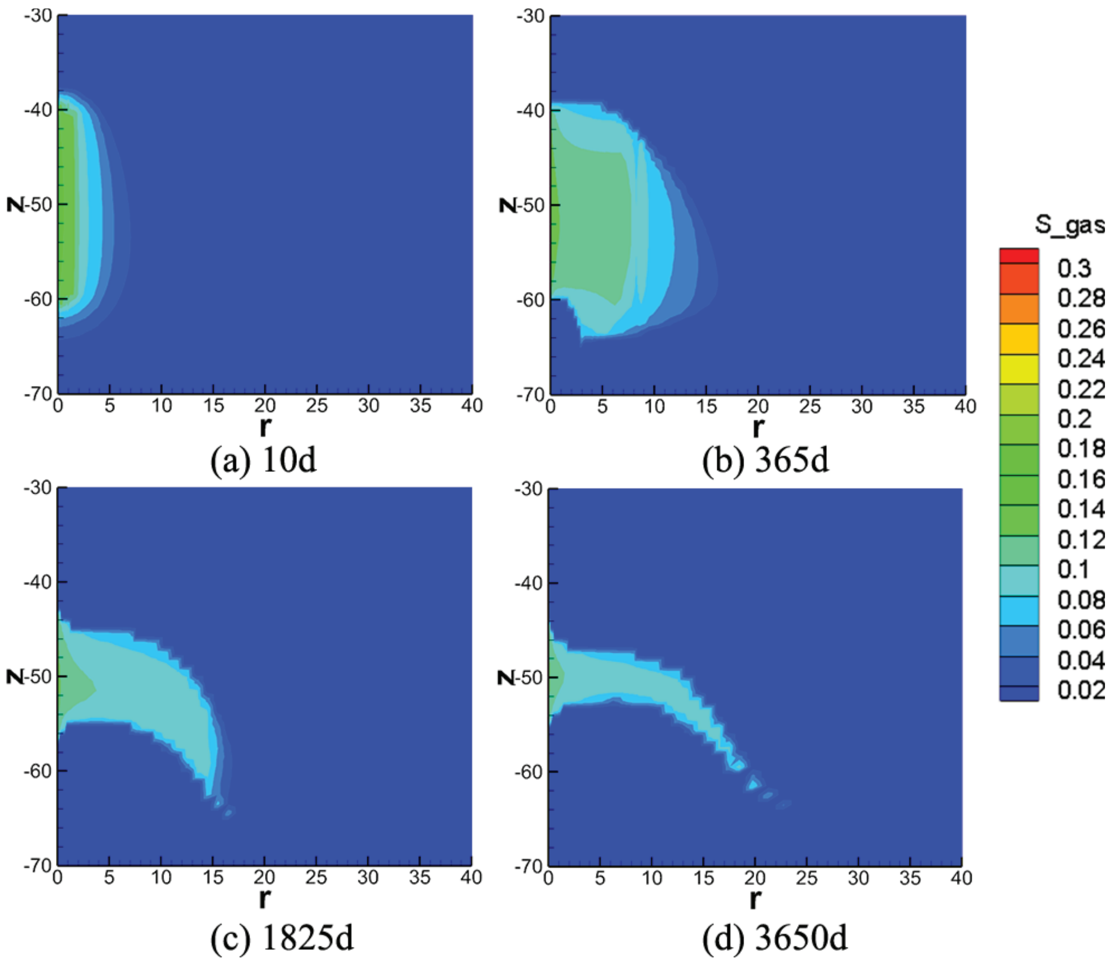

Figure 4: Evolution of gas saturation at different time periods.

from 1793, 1113, and 670 m^3/day to 341, 331, and 299 m^3/day, respectively. As time goes by, Q_W has increased significantly and the rate of increase has slowed down. The main reason for the increase of Q_W is that as the production proceeds, the area of hydrate decomposition increases, which leads to more and more water entering the production well. In the whole production, when the values of *n* are equal to 2.5, 3.5, and 4.5, Q_W increases from 75, 60, and 47 m^3/day to 205, 186, and 158 m^3/day, respectively.

Figure 6(a) shows that with the increase of *n*, the total CH_4 volume V_G and the total water volume V_W have decreased significantly. When *n* increases from 2.5 to 4.5, V_G drops from $1.93\times10^6 m^3$ to 1.34×10^6 m^3, and V_W drops from 6.69×10^5 m^3 to 4.46×10^5 m^3. When *n* = 4.5, the V_G and the V_W are 69% and 67% of *n* = 2.5, respectively.

Figure 6(b) gives the information about the change of gas-to-water ratio R_{GW} = V_P/V_W over time. Before 650 days, the R_{GW} gradually decreases as *n* increases. After 650 days, the R_{GW} values in three different cases are very close to each other. This phenomenon mainly stems from the fact that, in the later stage of production, as the

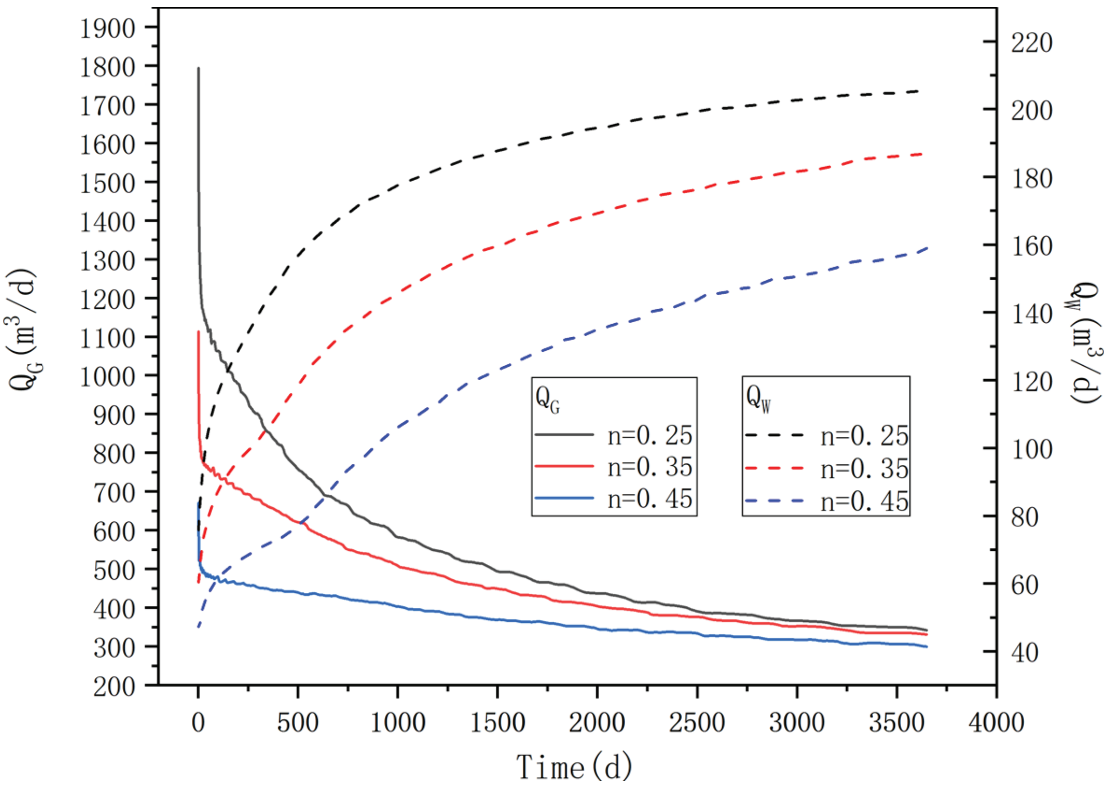

Figure 5: Evolution of Q_{PT} and Q_{PW} under three different *n* values.

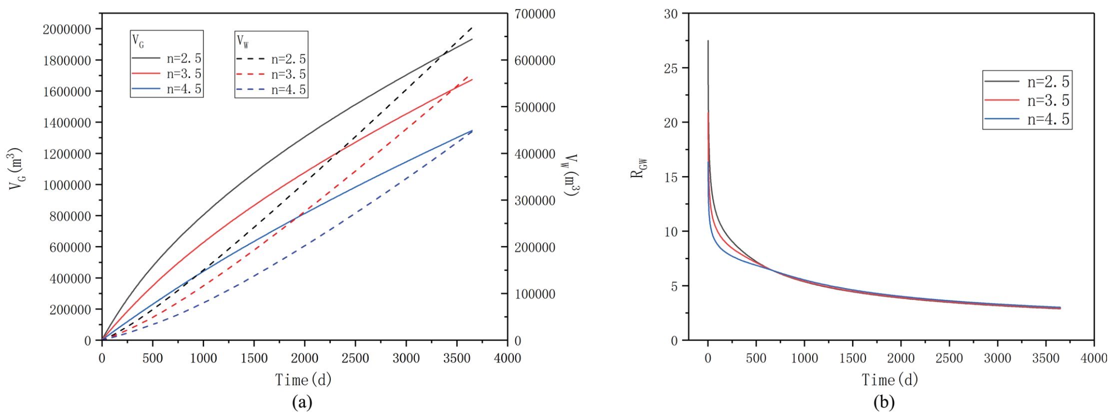

Figure 6: Evolution of V_G and V_W and gas–water ratio R_{GW} under three different *n* values.

decomposition front is far away from the production well, water and gas flowing into the production well tends to be stable, resulting in the same gas–water ratio in three different cases.

4. Conclusion

The effects of irreducible fluids saturation, such as irreducible water saturation and irreducible gas saturation, on gas hydrate production are studied in this article. The main conclusions can be drawn as follows. After 365th day, the water from the overburden and underburden enters the production well. In 10 years of production, the range of hydrate decomposition is within 30 meters. As *n* increases, both the Q_G and the Q_W increase. The reason is that the relative permeability of gas and water decrease rapidly with the decrease of saturation in higher *n*. In the early stage of production, as the *n* increases, the R_{GW} decreases. In the later stage, there is no effect on the R_{GW}.

Funding

This study has been supported by the National Natural Science Foundation of China (Grant No.51474112, Grant No.41502343).

References

[1] Uddin, M., Coombe, D., Law, D., et al. (2008). Numerical studies of gas hydrate formation and decomposition in a geological reservoir. *Journal of Energy Resources Technology-Transactions of the ASME*, vol. 130, no. 3, p. 032501.

[2] Li, X. S., Xu, C. G., Zhang, Y., et al. (2016). Investigation into gas production from natural gas hydrate: A review. *Applied Energy*, vol. 172, pp. 286–322.

[3] Lee, J., Park, S., and Sung, W. (2010). An experimental study on the productivity of dissociated gas from gas hydrate by depressurization scheme. *Energy Conversion and Management*, vol. 51, no. 12, pp. 2510–2515.

[4] Li, J., Qin, X., Qiu, H., et al. (2018). The first offshore natural gas hydrate production test in South China Sea. *China Geology*, vol. 1, pp. 5–19.

[5] Chen, L., Feng, Y. C., Okajima, J., et al. (2018). Production behavior and numerical analysis for 2017 methane hydrate extraction test of Shenhu, South China Sea. *Journal of Natural Gas Science and Engineering*, vol. 53, pp. 55–66.

[6] Su, Z., He, Y., Wu, N. Y., et al. (2012). Evaluation on gas production potential from laminar hydrate deposits in Shenhu Area of South China Sea through depressurization using vertical wells. *Journal of Petroleum Science and Engineering*, vol. 86–87, pp. 87–98.

[7] Li, G., Moridis, G. J., Zhang, K. N., et al. (2010). Evaluation of gas production potential from marine gas hydrate deposits in Shenhu Area of South China Sea. *Energy & Fuels*, vol. 24, no. 11, pp. 6018–6033.

[8] Jin, G. R., Xu, T. F., Xin, X., et al. (2016). Numerical evaluation of the methane production from unconfined gas hydrate-bearing sediment by thermal stimulation

and depressurization in Shenhu area, South China Sea. *Journal of Natural Gas Science and Engineering*, vol. 33, pp. 497–508.

[9] Sun, J. X., Zhang, L., Ning, F. L., et al. (2017). Production potential and stability of hydrate-bearing sediments at the site GMGS3-W19 in the South China Sea: A preliminary feasibility study. *Marine and Petroleum Geology*, vol. 86, pp. 447–473.

[10] Konno, Y., Fujii, T., Sato, A., et al. (2017). Key findings of the world's first offshore methane hydrate production test off the coast of Japan: Toward future commercial production. *Energy & Fuels*, vol. 31, no. 3, pp. 2607–2616.

[11] Su, Z., Huang, L., Wu, N. Y., et al. (2013). Effect of thermal stimulation on gas production from hydrate deposits in Shenhu area of the South China Sea. *Science China Earth Sciences*, vol. 56, no. 4, pp. 601–610.

[12] Moridis, G. J., Kowalsky, M. B., and Pruess, K. (2008). TOUGH+HYDRATE v1.0 User's Manual: A code for the simulation of system behavior in hydrate-bearing geologic media.

[13] Hatzikiriakos, S. G. and Englezos, P. (1993). The relationship between global warming and methane gas hydrates in the earth. *Chemical Engineering Science*, vol. 48, no. 23, pp. 3963–3969.